



Realizing the Harper Hamiltonian with Laser-Assisted Tunneling in Optical Lattices

Hirokazu Miyake, Georgios A. Siviloglou, Colin J. Kennedy, William Cody Burton, and Wolfgang Ketterle

*Research Laboratory of Electronics, MIT-Harvard Center for Ultracold Atoms, Department of Physics,
 Massachusetts Institute of Technology, Cambridge, Massachusetts 02139, USA*

(Received 6 August 2013; published 28 October 2013; publisher error corrected 28 October 2013)

We experimentally implement the Harper Hamiltonian for neutral particles in optical lattices using laser-assisted tunneling and a potential energy gradient provided by gravity or magnetic field gradients. This Hamiltonian describes the motion of charged particles in strong magnetic fields. Laser-assisted tunneling processes are characterized by studying the expansion of the atoms in the lattice. The band structure of this Hamiltonian should display Hofstadter's butterfly. For fermions, this scheme should realize the quantum Hall effect and chiral edge states.

DOI: [10.1103/PhysRevLett.111.185302](https://doi.org/10.1103/PhysRevLett.111.185302)

PACS numbers: 67.85.-d, 03.65.Vf, 03.75.Lm

Systems of charged particles in magnetic fields have led to many discoveries in science—including both the integer [1] and the fractional [2,3] quantum Hall effects—and have become important paradigms of quantum many-body physics [4]. Generalizations have led to important developments in condensed matter physics, including topological insulators [5,6], fractional Chern insulators [7,8], and Majorana fermions [9,10]. At high magnetic fields, exotic new phenomena like the fractal energy spectrum of Hofstadter's butterfly [11] are predicted to emerge. Its direct observation would require an inaccessibly high magnetic field of one flux quantum per unit cell—corresponding to ~ 10000 T in a traditional condensed matter system. Recently, some aspects of Hofstadter's butterfly were addressed using superlattices in high magnetic fields [12–15].

Neutral atoms provide an excellent platform to simulate the physics of charged particles in magnetic fields free from disorder. Rotating quantum gases realize the limit of weak magnetic fields, exploiting the equivalence between the Lorentz force and the Coriolis force. The observed vortex lattices [16,17] are analogous to magnetic flux lattices. A more general method to create synthetic magnetic fields for neutral atoms is based on the insight that vector potentials introduce spatially varying phases ϕ into the wave function when the particle propagates $\phi = \oint \mathbf{A} \cdot d\mathbf{s}/\hbar$, where the charge is included in the vector potential. For neutral atoms, such a phase structure can be realized through Berry phases, when two hyperfine states of the atom are coupled by Raman lasers with inhomogeneous intensity or detuning [18,19]. This concept of coupling of two or several internal states to realize synthetic magnetic fields was also suggested in optical lattice geometries [20–22]. Here, the crucial element is laser-assisted hopping between neighboring sites which imprints the phase of the laser into the atomic wave function. Alternatively, instead of using Raman laser beams, lattice modulation techniques can generate complex tunneling matrix elements in optical lattices [23,24]. Experimentally, these techniques have been used so far

only to realize staggered magnetic fields [24,25]. In the Munich experiment, the two internal states in the proposed schemes [20,22] were replaced by doubling the unit cell of the optical lattice using superlattices [25].

So far, all proposals for generating high magnetic fields are based on the coupling of different internal states. For alkali atoms, this involves different hyperfine states [20]. Spin flips between such states require near-resonant light which heats up the sample by spontaneous emission. At least for staggered fluxes, the realizations with lattice shaking and superlattices demonstrate that internal structure of the atom is not essential. Here, we suggest and implement a scheme which realizes the Harper Hamiltonian [26], a lattice model for charged particles in magnetic fields, the spectrum of which is the famous Hofstadter's butterfly [11]. Our scheme requires only far-off-resonant lasers and a single internal state. It is an extension of a scheme suggested by Kolovsky [27], which was shown to be limited to inhomogeneous fields [28], but as we show here, an additional momentum transfer in the laser-assisted hopping process provides a simple solution. While this work was in progress [29], an identical scheme was proposed by the Munich group [30]. In this Letter, we describe the features and implementation of this scheme, and characterize the laser-assisted hopping process.

We start with the simple Hamiltonian for noninteracting particles in a 2D cubic lattice

$$H = -\sum_{m,n} (J_x \hat{a}_{m+1,n}^\dagger \hat{a}_{m,n} + J_y \hat{a}_{m,n+1}^\dagger \hat{a}_{m,n} + \text{H.c.}), \quad (1)$$

where $J_{x(y)}$ describes tunneling in the x (y) direction and $\hat{a}_{m,n}^\dagger$ ($\hat{a}_{m,n}$) is the creation (annihilation) operator of a particle at lattice site (m, n) . Tunneling in the x direction is then suppressed by a linear tilt of energy Δ per lattice site, where Δ/h is the Bloch oscillation frequency. This tilt can be created with magnetic field gradients, gravity, or an ac Stark shift gradient. Resonant tunneling is restored with two far-detuned Raman beams of two-photon Rabi frequency Ω , frequency detuning $\delta\omega = \omega_1 - \omega_2$, and momentum transfer $\delta\mathbf{k} = \mathbf{k}_1 - \mathbf{k}_2$, as shown in Fig. 1(a).

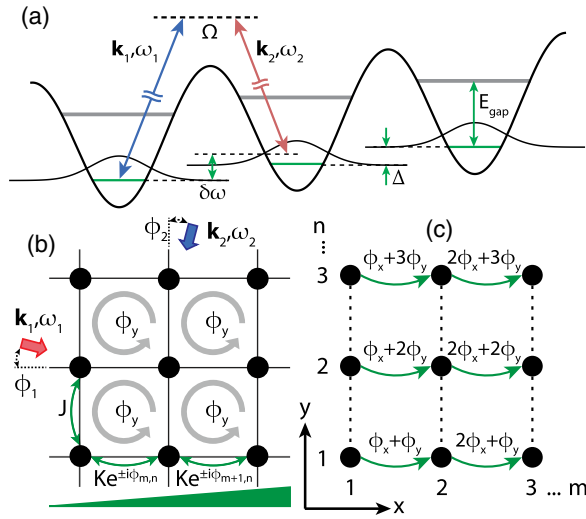


FIG. 1 (color online). (a) Raman-assisted tunneling in the lowest band of a tilted lattice with an energy offset Δ between neighboring sites and two-photon Rabi frequency Ω . (b) Experimental geometry to generate uniform magnetic fields using a pair of far-detuned laser beams and a uniform potential energy gradient. Tunneling along the x direction with amplitude K imprints a complex, spatially varying phase $\phi_{m,n}$ —with site indices (m, n) —into the system due to the momentum transfer in the y direction. (c) A schematic depicting the position-dependent phases of the tunneling process. The equivalent number of flux quanta per unit cell is $\alpha = \phi_y/2\pi$.

Note that the two Raman beams couple different sites but do not change the internal state of the atoms. For resonant tunneling $\delta\omega = \Delta/\hbar$, time averaging over rapidly oscillating terms [20] yields an effective Hamiltonian which is time independent. As a result, the tilt has disappeared because, in the dressed atom picture, site (m, n) with j and k photons in the two Raman beams is degenerate with site $(m+1, n)$ and $j+1$ and $k-1$ photons in the two beams. This effective Hamiltonian describes the system well, assuming that Δ is larger than the bandwidth $\sim J$ and smaller than the band gap E_{gap} . In addition, the effects of power broadening can be avoided if we choose Ω less than Δ . The resulting Hamiltonian is equivalent to one that describes charged particles on a lattice in a magnetic field under the tight-binding approximation [11,26]—the single-band Harper Hamiltonian

$$H = -\sum_{m,n} (K e^{-i\phi_{m,n}} \hat{a}_{m+1,n}^\dagger \hat{a}_{m,n} + J \hat{a}_{m,n+1}^\dagger \hat{a}_{m,n} + \text{H.c.}) \quad (2)$$

with a spatially varying phase $\phi_{m,n} = \delta\mathbf{k} \cdot \mathbf{R}_{m,n} = m\phi_x + n\phi_y$ where $\mathbf{R}_{m,n}$ denotes the position of each lattice site. Solutions in this model are periodic with respect to the number of flux quanta per unit cell α . If the frequencies of the Raman beams are similar to those used for the optical lattice, one can tune α over the full range between zero and one by adjusting the angle between the Raman beams, and consequently k_y . A similar Hamiltonian can be realized for the tunneling of phonons between ion microtraps [31].

The spatially dependent phase imprinted by the Raman lasers, given by $\phi_{m,n}$, can be intuitively understood in a perturbative regime, where $J_{\text{pert}} = J_y$ and

$$K_{\text{pert}} = \frac{\Omega}{2} \int d^2\mathbf{r} w^*(\mathbf{r} - \mathbf{R}_{m,n}) e^{-i\delta\mathbf{k} \cdot \mathbf{r}} w(\mathbf{r} - \mathbf{R}_{m,n} - a\hat{\mathbf{x}}) = K e^{-i\delta\mathbf{k} \cdot \mathbf{R}_{m,n}}. \quad (3)$$

Adding up the accumulated phases around a closed path, one sees that this method leads to an enclosed phase of $\phi_y = \delta k_y a$ per lattice unit cell of area a^2 , thus realizing the Harper Hamiltonian with $\alpha = \phi_y/2\pi$.

In a cubic lattice, the Wannier function $w(\mathbf{r})$ factorizes into $w(x)w(y)$ which are the localized Wannier-Stark and Wannier wave functions, respectively. The resulting expression for $K = (\Omega/2) \int dx w^*(x) e^{-ik_x x} w(x-a) \times \int dy w^*(y) e^{-ik_y y} w(y)$ shows that the momentum transfer in the x direction is necessary to have a nonvanishing tunneling matrix element K without changing the internal state. The x momentum transfer distinguishes our scheme from Refs. [20,22,27] and contributes to the vector potential $\mathbf{A} = [\hbar(k_y y + k_x x)/a]\hat{\mathbf{x}}$ but does not contribute to the enclosed flux or the value of the synthetic magnetic field \mathbf{B} . Note that this scheme does not realize the simple Landau gauge for the magnetic field.

For a more comprehensive description, we add the moving lattice— $V_{RM} = \Omega \sin(\delta\mathbf{k} \cdot \mathbf{r} - \omega t)$ —of the two Raman lasers along with a linear tilt to the Hamiltonian in Eq. (1). In addition to the off-diagonal laser-assisted tunneling term, this moving lattice causes a diagonal term, which is a temporal modulation of the on-site energies. A unitary transformation, as in Refs. [29,32], leads to a frame rotating nonuniformly in time and position that eliminates the diagonal time dependence. For resonant drive $\Delta = \hbar\delta\omega$, the on-site energies are all equal and vanish while the remaining off-diagonal coupling has a time-independent part, leading to the Harper Hamiltonian, as in Eq. (2). The resulting expressions for K and J are (see the Supplemental Material [33])

$$K = \Omega \Phi_{y0} \left[\Phi_{x1} \frac{J_1(\Gamma_x)}{\Gamma_x} + i\Phi'_{x1} \frac{dJ_1(\Gamma_x)}{d\Gamma_x} \right], \quad (4)$$

$$J = J_y J_0(\Gamma_y), \quad \Gamma_i = \frac{2\Omega \Phi_{y0} \Phi_{x0}}{\Delta} \sin\left(\frac{k_i a}{2}\right),$$

where $\Phi_{i0} = \langle 0 | \cos(k_i x_i) | 0 \rangle$ is the on-site matrix element, and $\Phi_{x1} = \langle 0 | \sin[k_x(x-a/2)] | 1 \rangle$ and $\Phi'_{x1} = \langle 0 | \cos[k_x(x-a/2)] | 1 \rangle$ are the off-diagonal matrix elements. This result is more general than the case of phase modulation [32] and the tight-binding limit in Refs. [30,34], where K is proportional to $J_1(x)$.

We implement the Harper Hamiltonian with each Raman laser aligned along one of the two lattice directions x and y corresponding to momentum transfer in both directions of $\hbar k_L$ —the single-photon recoil of the lattice laser. The magnetic flux per unit cell resulting from $k_y = k_L$ is $\alpha = 1/2$. In the tight-binding limit for this momentum transfer, $\Phi_{i0} \approx 1$

and $\Phi_{x1} \approx -2J_x/\Delta \gg \Phi'_{x1}$, so the resonant tunneling amplitudes resulting from $k_x = k_L$ simplify to

$$K = J_x J_1 \left(\frac{2\Omega}{\Delta} \right) \quad \text{and} \quad J = J_y J_0 \left(\frac{2\Omega}{\Delta} \right). \quad (5)$$

Experimentally, the system is prepared by starting with a Bose-Einstein condensate of $\sim 5 \times 10^5$ ^{87}Rb atoms in the $|2, -2\rangle$ state in a crossed dipole trap. The Raman lasers are ramped up to their final intensities in 30 ms at a large detuning of 200 kHz and are switched to their final detuning after the tilt is applied to the system (see below). Unwanted interferences between lattice and Raman lasers are avoided with relative frequency offsets of >30 MHz using acousto-optic modulators. Next, we adiabatically load the condensate in 100 ms into a two-dimensional cubic optical lattice of spacing $\lambda_{\text{latt}}/2 = 532$ nm. For longer hold times, a weak $2E_r$ lattice beam along the third direction is simultaneously ramped up to provide additional confinement. Here, $E_r = \hbar^2 k_L^2/2m \approx h \times 2$ kHz is the single-photon recoil energy. The two-photon Rabi frequency of the moving Raman lattice is determined using free-space Rabi oscillations and chosen to be considerably smaller than the static lattice.

After loading the condensate into the lattice, a uniform potential energy gradient of $mga/h \approx 1.1$ kHz between adjacent lattice sites is applied by turning off the confining crossed dipole traps in 20 ms. Alternatively, we have successfully used a magnetic field gradient to access a broader range of tilts. The gravitational gradient has the advantage of a much faster switching time compared to the magnetic gradient. The cloud widths σ_x and σ_y are obtained by standard absorption imaging along the direction perpendicular to the 2D lattice.

The essential feature of our implementation of the Harper Hamiltonian is that tunneling in the x direction is suppressed by a potential tilt and reestablished by laser-assisted tunneling. This is demonstrated in Fig. 2, which shows the resonance for the laser-assisted process. For this,

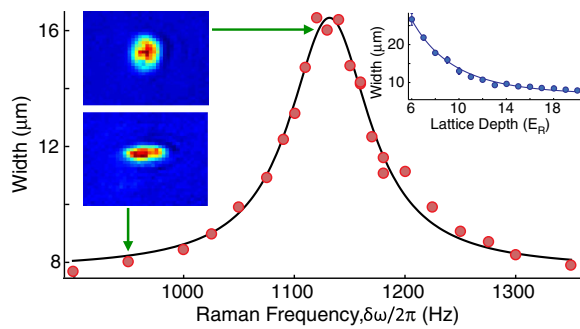


FIG. 2 (color online). *In situ* cloud width as a function of Raman detuning $\delta\omega$ after an expansion of 500 ms, with a Raman lattice depth of $\Omega = \Delta/4$. The solid line is a Lorentzian fit to the experimental data (dots) centered at 1133 Hz—consistent with the gravitational offset between sites. Pictures (of size $135 \times 116 \mu\text{m}$) show typical column densities on or off resonance. Inset: Dependence of the laser-assisted tunneling on optical lattice depth.

tunneling is characterized by looking at the expansion of the cloud within the lattice. Expansion occurs since the confinement by the optical dipole trap has been switched off, and due to some heating during the 500 ms hold time. Note that for fully coherent time evolution, charged particles in a magnetic field will undergo cyclotron motion which would suppress the expansion. The resonance width of 60 Hz may have contributions from laser frequency jitter, inhomogeneous lattice potential, and atomic interactions. The Lorentzian fit suggests a homogenous broadening mechanism.

The dependence of K and J on the intensity of the Raman lasers (described by Bessel functions) allows tuning of the ratio of the two. For low intensities, K increases linearly with the intensity, and J decreases quadratically. The latter reflects the depletion of the unperturbed Wannier function by the modulation due to the moving Raman lattice. Figure 3(a) shows experimental results in qualitative agreement with these predictions.

For a quantitative interpretation of the expansion of the cloud, we assume an incoherent diffusion process, where the square of the width σ of the expanded cloud is proportional to the tunneling rate times expansion time. For short times, the expansion of the cloud should be fully coherent, and the width should increase linearly with time. However, heating by light scattering and intensity fluctuations of the

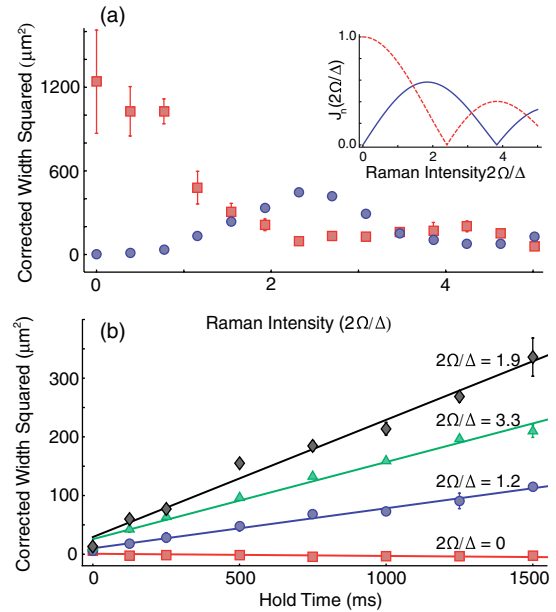


FIG. 3 (color online). (a) Expansion as a function of resonant Raman laser intensity shows the laser-assisted tunneling along the tilt direction (blue circles) and the tunneling rate J along the transverse direction (red squares). Data taken at lattice depths of $9E_r$ and hold time of 1500 ms. Inset: Theoretical prediction for the tunneling rates K and J in terms of Bessel functions [Eq. (5)]. (b) Time evolution of the squared width for different Raman laser intensities. From the slope of the lines, we obtain the laser-assisted tunneling rates and their statistical errors: 0.2 ± 0.08 (red squares), 4 ± 0.5 (blue circles), 12 ± 1 (black diamonds), and 8 ± 0.5 Hz (blue triangles).

laser beams lead to an incoherent, diffusive expansion. For finite time, we correct for the initial size σ_0 by assuming that the expansion and initial size add in quadrature, and plot the corrected squared width $\sigma_{\text{corr}}^2 = \sigma^2 - \sigma_0^2$ versus time. The slope is proportional to the laser-assisted tunneling rate. Absolute tunneling rates are obtained by comparing this result to the expansion of the cloud in the y direction with the Raman beams far off resonance, when normal tunneling occurs. The ratio of the slopes is then K/J_y , with J_y calculated from the calibrated lattice depth to be $\sim \hbar \times 48$ Hz. Figure 3(b) shows the time evolution of the square of the corrected size for various Raman intensities. The linear fits support the assumption of incoherent diffusion and allow a determination of tunneling rates, as summarized in the figure caption.

Laser-assisted tunneling is a powerful tool to manipulate the motion of atoms in optical lattices and to create novel Hamiltonians. We now describe different tunneling processes observed by a wide scan of the Raman detuning, shown in Fig. 4. A strong peak near 568 Hz fulfills the resonance condition $2\delta\omega = \Delta/\hbar$ for a four-photon nearest-neighbor tunneling process. This resonance is similar to the one observed in Ref. [35] by shaking the lattice. Note that the four-photon resonance is narrower (20 Hz versus 60 Hz) than the two-photon resonance, indicative of a higher-order process. Broad features at even lower frequency are most likely due to higher-order tunneling resonances and low-lying excitations within the first band.

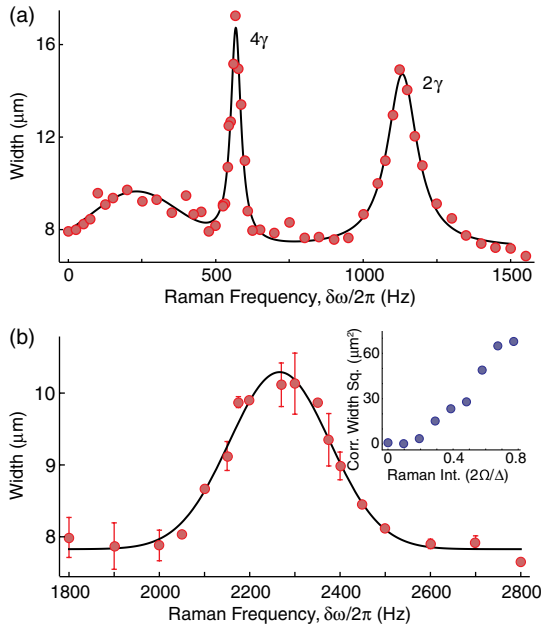


FIG. 4 (color online). Spectrum of excitations and tunneling resonances. (a) A strong, four-photon, nearest-neighbor tunneling resonance appears at $\Delta/2\hbar$ along with the K resonance at Δ/\hbar . These data were taken at a lattice depth of $9E_r$, for a two-photon Raman Rabi frequency of 1092 Hz and 500 ms expansion time. (b) Observation of next-nearest-neighbor laser-assisted tunneling at 2Δ and the expansion of the cloud as a function of Ω . Inset: No saturation is reached. Expansion time of 1500 ms.

Next-nearest-neighbor tunneling occurs at $\delta\omega = 2\Delta/\hbar$, twice the frequency of the fundamental resonance. For a shaken lattice (no Raman beams), this was studied in Ref. [36]. Analyzing the expansion of the cloud gives a tunneling rate of 0.4 ± 0.1 Hz, comparable to the next-nearest-neighbor tunneling rate in an untilted lattice, ~ 0.8 Hz in our system. However, in an untilted lattice, next-nearest-neighbor tunneling is typically a hundred times slower than nearest-neighbor tunneling, whereas in laser-assisted tunneling, the two processes can be independently controlled by the laser power at the two resonant frequencies. Tunneling rates below 1 Hz are too slow for pursuing many-body physics, but the same scheme can be implemented for lighter atoms such as lithium in a shorter wavelength lattice, where the relevant scale factor, the recoil energy, is increased by a factor of 50.

After realizing and characterizing all parts of the Harper Hamiltonian, the next goal is to map out its band structure as a function of quasimomentum and magnetic field α —the Hofstadter butterfly. The ground state for a given α should be accessible by adiabatically transferring a condensate into this Hamiltonian. The ground state of the Harper Hamiltonian for $\alpha = 1/2$ has a clear signature in that its magnetic unit cell is twice as large as the lattice unit cell and its wave function has a unit cell that is 4 times as large, so time of flight imaging will reveal the resulting reduction of the Brillouin zone in momentum space by a factor of 4 [25,29,37–39]. So far, we have not been able to preserve the low entropy of the initial condensate and observe the ground state.

Preliminary experiments have shown less heating by the Raman beams at larger frequency detuning, requiring larger magnetic field gradients. An optimum detuning should be near half the band gap, avoiding inter- and intraband transitions. Possibly, an extension of the treatment of light scattering in optical lattices [40] could predict if there is a fundamental lower limit to the ratio of heating rate over K . Another potential source of heating is atomic interactions. Instabilities of certain quasimomentum states in optical lattices have been studied in Refs. [41,42]. Interaction-induced heating effects can in principle be avoided by using Feshbach resonances to tune the scattering length to zero or by using a single spin component of a fermionic gas. Once the ground state of the Harper Hamiltonian is established, different quasimomentum states can be populated through Bloch oscillations which occur at frequency $\delta = \delta\omega - \Delta/\hbar$, when the Raman lasers are slightly detuned from the resonance studied here.

The Harper Hamiltonian established in this work will be the starting point for many exciting explorations, including the quantum Hall effect, Dirac points, and novel topological phenomena [8,43]. Interactions between atoms may also lead to bosonic Laughlin states [44] and nonlinear Hofstadter eigenmodes [45]. The lowest band is topologically nontrivial with a Chern number of 1 [46] and should show chiral edge states. Most importantly, our scheme is simpler and potentially more robust than other suggestions,

since it does not require near-resonant light for connecting hyperfine states. It can be implemented for any atom—including the workhorse fermionic atoms lithium and potassium—which has small fine structure splittings, making it impossible to couple different spin states with negligible heating by spontaneous emission.

We acknowledge Yuri Lensky for experimental assistance. We thank Wujie Huang for helpful discussions and critical reading of the manuscript. This work was supported by the NSF through the Center of Ultracold Atoms, by NSF Grant No. PHY-0969731; under ARO Grant No. W911NF-13-1-0031 with funds from the DARPA OLE Program; and by ONR.

Note added.—Recently, we became aware of similar work carried out by Bloch and co-workers [34].

-
- [1] K. von Klitzing, G. Dorda, and M. Pepper, *Phys. Rev. Lett.* **45**, 494 (1980).
- [2] D. C. Tsui, H. L. Stormer, and A. C. Gossard, *Phys. Rev. Lett.* **48**, 1559 (1982).
- [3] R. B. Laughlin, *Phys. Rev. Lett.* **50**, 1395 (1983).
- [4] M. Lewenstein, A. Sanpera, and V. Ahufinger, *Ultracold Atoms in Optical Lattices* (Oxford University Press, Oxford, England, 2012).
- [5] C. L. Kane and E. J. Mele, *Phys. Rev. Lett.* **95**, 226801 (2005).
- [6] M. König, S. Wiedmann, C. Brüne, A. Roth, H. Buhmann, L. W. Molenkamp, X.-L. Qi, and S.-C. Zhang, *Science* **318**, 766 (2007).
- [7] N. Regnault and B. A. Bernevig, *Phys. Rev. X* **1**, 021014 (2011).
- [8] G. Möller and N. R. Cooper, *Phys. Rev. Lett.* **103**, 105303 (2009).
- [9] L. Fu and C. L. Kane, *Phys. Rev. Lett.* **100**, 096407 (2008).
- [10] V. Mourik, K. Zuo, S. M. Frolov, S. R. Plissard, E. P. A. M. Bakkers, and L. P. Kouwenhoven, *Science* **336**, 1003 (2012).
- [11] D. R. Hofstadter, *Phys. Rev. B* **14**, 2239 (1976).
- [12] B. Hunt, J. D. Sanchez-Yamagishi, A. F. Young, M. Yankowitz, B. J. LeRoy, K. Watanabe, T. Taniguchi, P. Moon, M. Koshino, P. Jarillo-Herrero, and R. C. Ashoori, *Science* **340**, 1427 (2013).
- [13] L. Ponomarenko, R. V. Gorbachev, G. L. Yu, D. C. Elias, R. Jalil, A. A. Patel, A. Mishchenko, A. S. Mayorov, C. R. Woods, J. R. Wallbank, M. Mucha-Kruczynski, B. A. Piot, M. Potemski, I. Grigorieva, K. S. Novoselov, F. Guinea, V. I. Falko, and A. K. Geim, *Nature (London)* **497**, 594 (2013).
- [14] C. R. Dean, L. Wang, P. Maher, C. Forsythe, F. Ghahari, Y. Gao, J. Katoch, M. Ishigami, P. Moon, M. Koshino, T. Taniguchi, K. Watanabe, K. L. Shepard, J. Hone, and P. Kim, *Nature (London)* **497**, 598 (2013).
- [15] C. Albrecht, J. H. Smet, K. von Klitzing, D. Weiss, V. Umansky, and H. Schweizer, *Phys. Rev. Lett.* **86**, 147 (2001).
- [16] K. W. Madison, F. Chevy, W. Wohlleben, and J. Dalibard, *Phys. Rev. Lett.* **84**, 806 (2000).
- [17] J. R. Abo-Shaer, C. Raman, J. M. Vogels, and W. Ketterle, *Science* **292**, 476 (2001).
- [18] Y.-J. Lin, R. L. Compton, K. Jimenez-Garcia, J. V. Porto, and I. Spielman, *Nature (London)* **462**, 628 (2009).
- [19] J. Dalibard, F. Gerbier, G. Juzeliūnas, and P. Öhberg, *Rev. Mod. Phys.* **83**, 1523 (2011).
- [20] D. Jaksch and P. Zoller, *New J. Phys.* **5**, 56 (2003).
- [21] E. J. Mueller, *Phys. Rev. A* **70**, 041603 (2004).
- [22] F. Gerbier and J. Dalibard, *New J. Phys.* **12**, 033007 (2010).
- [23] J. Struck, C. Ölschläger, M. Weinberg, P. Hauke, J. Simonet, A. Eckardt, M. Lewenstein, K. Sengstock, and P. Windpassinger, *Phys. Rev. Lett.* **108**, 225304 (2012).
- [24] J. Struck, M. Weinberg, C. Ölschläger, P. Windpassinger, J. Simonet, K. Sengstock, R. Höppner, P. Hauke, A. Eckardt, M. Lewenstein, and L. Mathey, *Nat. Phys.*, doi: 10.1038/nphys2750 (2013).
- [25] M. Aidelsburger, M. Atala, S. Nascimbène, S. Trotzky, Y.-A. Chen, and I. Bloch, *Phys. Rev. Lett.* **107**, 255301 (2011).
- [26] P. G. Harper, *Proc. Phys. Soc. London Sect. A* **68**, 874 (1955).
- [27] A. R. Kolovsky, *Europhys. Lett.* **93**, 20003 (2011).
- [28] C. E. Creffield and F. Sols, *Europhys. Lett.* **101**, 40001 (2013).
- [29] H. Miyake, Ph.D. thesis, Massachusetts Institute of Technology, 2013.
- [30] M. Aidelsburger, M. Atala, S. Nascimbène, S. Trotzky, Y.-A. Chen, and I. Bloch, *Appl. Phys. B*, doi: 10.1007/s00340-013-5418-1 (2013).
- [31] A. Bermudez, T. Schaetz, and D. Porras, *Phys. Rev. Lett.* **107**, 150501 (2011).
- [32] M. G. Tarallo, A. Alberti, N. Poli, M. L. Chiofalo, F.-Y. Wang, and G. M. Tino, *Phys. Rev. A* **86**, 033615 (2012).
- [33] See Supplemental Material at <http://link.aps.org/supplemental/10.1103/PhysRevLett.111.185302> for a detailed derivation of the Harper Hamiltonian from the Wannier-Stark Hamiltonian with laser-assisted hopping.
- [34] M. Aidelsburger, M. Atala, M. Lohse, J. T. Barreiro, B. Paredes, and I. Bloch, preceding Letter, *Phys. Rev. Lett.* **111**, 185301 (2013).
- [35] C. Sias, H. Lignier, Y. P. Singh, A. Zenesini, D. Ciampini, O. Morsch, and E. Arimondo, *Phys. Rev. Lett.* **100**, 040404 (2008).
- [36] V. V. Ivanov, A. Alberti, M. Schioppo, G. Ferrari, M. Artoni, M. L. Chiofalo, and G. M. Tino, *Phys. Rev. Lett.* **100**, 043602 (2008).
- [37] G. Möller and N. R. Cooper, *Phys. Rev. A* **82**, 063625 (2010).
- [38] T. P. Polak and T. A. Zaleski, *Phys. Rev. A* **87**, 033614 (2013).
- [39] S. Powell, R. Barnett, R. Sensarma, and S. Das Sarma, *Phys. Rev. A* **83**, 013612 (2011).
- [40] H. Pichler, A. J. Daley, and P. Zoller, *Phys. Rev. A* **82**, 063605 (2010).
- [41] L. Fallani, L. De Sarlo, J. E. Lye, M. Modugno, R. Saers, C. Fort, and M. Inguscio, *Phys. Rev. Lett.* **93**, 140406 (2004).
- [42] G. K. Campbell, J. Mun, M. Boyd, E. W. Streed, W. Ketterle, and D. E. Pritchard, *Phys. Rev. Lett.* **96**, 020406 (2006).
- [43] S. Powell, R. Barnett, R. Sensarma, and S. Das Sarma, *Phys. Rev. A* **83**, 013612 (2011).
- [44] A. S. Sørensen, E. Demler, and M. D. Lukin, *Phys. Rev. Lett.* **94**, 086803 (2005).
- [45] O. Manela, M. Segev, D. N. Christodoulides, and D. Kip, *New J. Phys.* **12**, 053017 (2010).
- [46] M. Hafezi, A. S. Sørensen, E. Demler, and M. D. Lukin, *Phys. Rev. A* **76**, 023613 (2007).